# KINEMATIC, AERODYNAMIC AND ANATOMICAL MECHANISMS IN THE SLOW, MANEUVERING FLIGHT OF PIGEONS

DOUGLAS R. WARRICK* AND KENNETH P. DIAL

*Division of Biological Sciences, University of Montana, Missoula, MT 59812-1002, USA*

*e-mail: drw@selway.umt.edu

## Summary

A high-speed (200 Hz) infrared video system was used in a three-dimensional analysis of pigeon wing and body kinematics to determine the aerodynamic and anatomical mechanisms they use to produce force asymmetries to effect a turn during slow ($3\,\mathrm{m\,s^{-1}}$) flight. Contrary to our expectations, pigeons used downstroke velocity asymmetries, rather than angle of attack or surface area asymmetries, to produce the disparities in force needed for directional changes. To produce a bank, a velocity asymmetry is created early in the downstroke and, in the majority of cases, then reversed at the end of the same downstroke, thus arresting the rolling angular momentum. When the velocity asymmetry was not reversed at the end of downstroke, the arresting force asymmetry was produced during upstroke, with velocity asymmetries creating disparate drag forces on the wings. Rather than using subtle aerodynamic variables to produce subtle downstroke force asymmetries, pigeons constantly adjust their position using a series of large alternating and opposing forces during downstroke and upstroke. Thus, a pigeon creates a precise 'average' body position (e.g. bank angle) and flight path by producing a series of rapidly oscillating movements. Although the primary locomotor event (downstroke) is saltatory, maneuvering during slow flight should be considered as a product of nearly continuous, juxtaposed force generation throughout the wingbeat cycle. Further, viewing upstroke as more than stereotypical, symmetrical wing recovery alters the evolutionary and functional context of investigations into the musculoskeletal mechanisms and the associated neural control involved in this unique kinematic event.

Key words: pigeon, *Columba livia*, three-dimensional kinematics, flight, maneuvering, slow flight.

## Introduction

While the high mass-specific power requirements of slow flight have undoubtedly been a strong selective pressure in the evolution of avian flight anatomy (e.g. the keel, the pectoralis), such structures would be of little use without the concomitant evolution of mechanisms that allow maneuvering during slow flight. In concert, the abilities to fly slowly and to maneuver precisely have important ecological and evolutionary ramifications. Birds lacking such abilities (e.g. albatross) are committed to spatially large breeding and foraging habitats. Conversely, the ability of some taxa (e.g. the passerines) to fly slowly and precisely, and thus utilize a wide range of spatial habitats, has been suggested as the evolutionary primer allowing for their explosive diversification (Warrick *et al.* 1998). Addressing this hypothesis first requires a knowledge of what structures are involved in slow maneuvering flight. The broad purpose of the present study is to provide insight into what those structures are.

The fundamental mechanism used to maneuver during slow or fast flight is the same: the two wings must generate disparate aerodynamic forces. Of the variables combining to produce the lifting force, relative incident air velocity over the wing ($V_{ri}$), the lift coefficient and the surface area of the wing are available

to a bird as means of producing lift force asymmetry. A bird could produce a force asymmetry by creating asymmetry in downstroke velocities; lift coefficient could be altered differentially by pronation or supination of the wings to create asymmetry in angle of attack, and the surface area of the wings could be altered asymmetrically by flexion at the wrist and/or elbow. As lift increases with the square of velocity, but only linearly with changes in lift coefficient and surface area, one might expect birds to use alterations in these latter two variables to produce the fine-scale asymmetries needed for subtle directional changes during slow flight. Further, as upstroke is thought to be aerodynamically inactive (Rayner, 1988), the need to create controllable asymmetries would seem to be critical; with nothing to arrest the momentum of a large force asymmetry produced during downstroke, a bird would roll unabated during upstroke. However, other kinematic studies have concluded that an aerodynamic force might be produced during upstroke (Brown, 1948; Norberg, 1976; Aldridge, 1986) and therefore used in some manner during maneuvering. The purpose of the present study is to infer, through kinematics, what aerodynamic and anatomical mechanisms birds use when effecting a turn during low-speed flight.
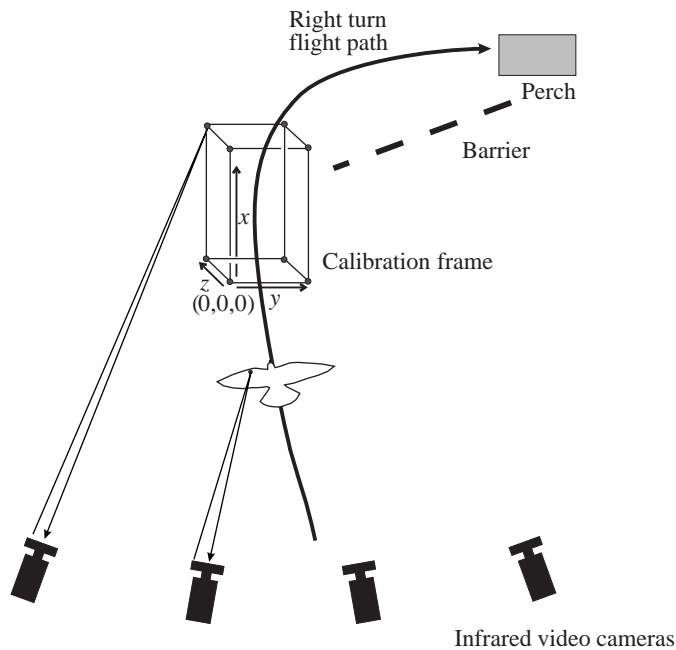
Fig. 1. Recording apparatus, flight path and three-dimensional coordinate ($x,y,z$) space. Maintaining the same height above the floor, the birds performed right or left turns to maneuver around a barrier. The calibration frame was removed after the cameras had been calibrated. The pigeons were in view of the cameras for 2–4 wingbeats at the beginning to intermediate part of the turn (approximately where the calibration frame had been located).

## Materials and methods

### Bird training and flight corridor

Three rock pigeons (*Columba livia* Gmelin; hereafter referred to as pigeons) were captured in Missoula, Montana, USA, and housed in the University of Montana's animal facility, where they were provided with food and water *ad libitum*. The birds were trained to take-off from the hand, maneuver around a barrier, and fly to a perch. The barrier consisted of a 2.5 m×3 m net curtain (gardener's anti-bird netting) that was clearly visible to the birds but did not obscure them from view of the tracking cameras (Fig. 1). The net curtain and perch could be moved to create a right- or left-hand turn without requiring movement of the tracking cameras. The birds were released at perch height (≈1.5 m), and thus did not need to change altitude to complete the flight. Birds were motivated to expedite the flight to the perch by placing a pigeon of the opposite sex in a cage next to the perch.

Kinematic data were collected from 10 right-hand and 10 left-hand turning flights for each pigeon and combined for analysis.

### Three-dimensional coordinate mapping

Body position coordinates were calculated using commercially available hardware and software (Motion Analysis Corporation) developed for the study of motion in three dimensions. The system consisted of a video processing unit capable of converting simultaneous images from multiple cameras into digital images that could then be tracked through a calibrated three-dimensional coordinate space. Four infra-red cameras (200 Hz sampling rate) were used to triangulate and track markers on the birds. Each camera produced infrared light that was reflected back to the cameras by markers on the birds; as cameras gathered only infrared light, only the images of the markers on the birds were converted to digital data by the video processor. The three-dimensional coordinate space was established by least-squares estimation of coefficients (11 per camera view) that described the position of each camera in the *x*, *y* and *z* dimensions relative to the known coordinates of control points. The eight non-coplanar control points used for calibration were located on a standard calibration frame (78.70 cm×74.85 cm×50.14 cm; Fig. 1) provided by Motion Analysis Corporation. These coefficients were then used in a direct linear transformation which mapped the coordinate position of each bird marker.

The four cameras were mounted 3 m off the ground and approximately 1 m apart. The calibration frame was placed in the portion of the flight path of greatest interest (entry and early portion of the turn). The average of the distances from the cameras to the calibration frame was 370 cm, and the cameras were pointed such that the calibration frame filled large portions of their fields of view. Limiting the field of view to only the space between the control points reduced the need for extrapolation of coordinates beyond the calibrated space and reduced errors due to camera lens aberration. Cameras were calibrated before each data-collection session and judged for precision on the basis of the 'norm of residuals', a standard developed by Motion Analysis Corporation for their system. A maximum normed residual greater than 0.25 was considered a poor calibration; that is, it would produce unacceptable error in subsequent coordinate mapping (Motion Analysis Corporation, 1991). The largest maximum normed residual for any calibration was 0.2 (range 0.08–0.20, mean 0.12).

Using a rigid, artificial 'wing' equipped with markers analogous to those on the bird test subjects, we conducted tests to determine the precision of the coordinate mapping system. The distances between the six markers on the artificial wing ranged from 5.55 to 21.05 cm. The wing was moved by hand through the coordinate space on a path similar to those taken by the birds, while varying its presentation angle and speed to emulate a flapping bird wing. The distances between the points on the wing obtained from the Motion Analysis System were then compared with the distances as measured by a ruler. Mean distances on the artificial wing as measured by the Motion Analysis System ($N$=1009) were within an average of 0.4 % of the distances as measured by ruler. More importantly, the standard deviations of the mean distances obtained from the system ranged from 0.115 to 0.286 cm; in other words, 95 % of the distance values were within 2 % of the means. Overall, we estimate an error of 2.5–3.0 % in our coordinate mapping.

Six points were tracked on the birds' wings: left tip (*LT*), left wrist (*LW*), left trailing edge (*LR*), right tip (*RT*), right wrist (*RW*) and right trailing edge (*RR*). Three body markers were also tracked: anterior (*A*), left (*L*) and right (*R*) (Fig. 2A).
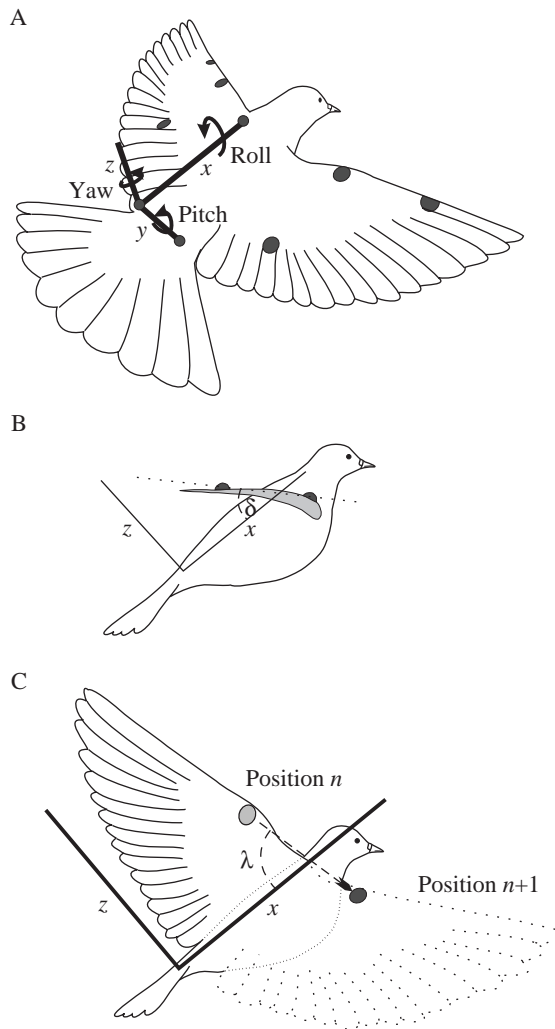
Fig. 2. (A) Positions of the infrared-reflective markers on the pigeons. The three body markers allowed the creation of a local *x*, *y*, *z* coordinate system on the bird, allowing kinematic measurements to be calculated relative to the body. The three traditional axes of rotation for a 'flying machine' are labeled on the local coordinate system. (B) Pronation angle ($\delta$) during the downstroke. (C) Downstroke angle ($\lambda$).

Because of the large inertial and drag forces created by the distal wing, wingtip markers were limited to a round, self-adhesive reflective sticker (0.2 g, 2.5 cm diameter) placed approximately half-way down the shaft of the last primary feather, just distal to the primary coverts and wrapped around the leading edge. The resulting flat marker presented little or no drag area and was generally ignored by the birds. However, the flat marker could be seen only at mid-to-late downstroke for 4–5 frames (20–25 ms), resulting in a relative paucity of positional data for the wingtips. The more proximal positions of the wrist and trailing-edge markers allowed the use of a more visible hemispherical reflective 'wart' – a small piece of low-density styrene packing material covered with reflective tape. The resulting marker was 1 cm in diameter and had a mass of 0.3 g. The warts were sewn to small pieces of surgical tape,

which were then fixed to the dorsal surface of the wrist, directly behind the depression in the leading edge of the wrist joint produced by the articulation of the first digit and the carpals. The trailing-edge marker was placed approximately half-way (approximately 7 cm) down the shaft of the secondary feathers, such that a line drawn between the wrist marker and the trailing-edge marker would be perpendicular to the leading edge of the wing when fully extended. The slightly raised nature of the warts seemed to have no impact of the flight behavior of the pigeons, although it necessitated some fine adjustments in calculation of angle of attack (see below and Appendix). The three body markers were reflective spheres (2.0 g, 1.3 cm diameter) attached to a cloth backpack held to the bird by elastic straps.

The cameras were positioned approximately 1.75 m above the flight path of the birds; with the birds flying away from the cameras, this position afforded the best view of the wings' dorsal reflective markers during downstroke. With the field of view of the cameras limited to approximately 1 m³, the birds were in view for 0.5–0.75 s of each flight, allowing 3–5 downstrokes to be tracked per trial. To map the coordinate position of a marker at a given instant, the marker had to be within view of at least two cameras; failing this, gaps would occur in the three-dimensional paths. Because the dorsal surfaces of the wings were close together during the top of upstroke and early downstroke (approximately the first 10° of the downstroke arc), the wing markers were obscured from the view of the cameras for these portions of the wingbeat cycle. For the remainder of the downstroke, only extremely rare sampling gaps of two or fewer consecutive sampling points ($\leqslant$10 ms) occurred for the wrist, trailing-edge and body markers. Such gaps were filled using cubic spline interpolation. The flat wingtip markers were generally not visible until the wings approached a presentation perpendicular to the cameras during approximately the middle 50% of downstroke. Because of the pronounced supination of the wing during upstroke, for this portion of the wingbeat cycle the dorsal markers were in the view of the overhead cameras for only a small portion of the flight path. However, 13 upstrokes were tracked to the standards of the tracked downstrokes.

Raw three-dimensional coordinate series for each trial were smoothed using a two-pass, fourth-order Butterworth smoothing algorithm (Motion Analysis Corporation, 1991) with a frequency cut-off of 5 Hz. Smoothed coordinate positions were used to calculate the kinematic variables.

### Calculation of kinematic variables in the laboratory coordinate system: flight speed, turning radius and curvature, angle of attack

Calibration of the cameras to the frame standard created a three-dimensional coordinate system through which the birds flew, executing either right or left turns (Fig. 1). Owing to the precision of the recording equipment, after smoothing, the positional data were clean enough to allow direct derivation of flight speed. Using the position of the anterior body marker (*A*), flight speed (*S*) was defined as the change in position from
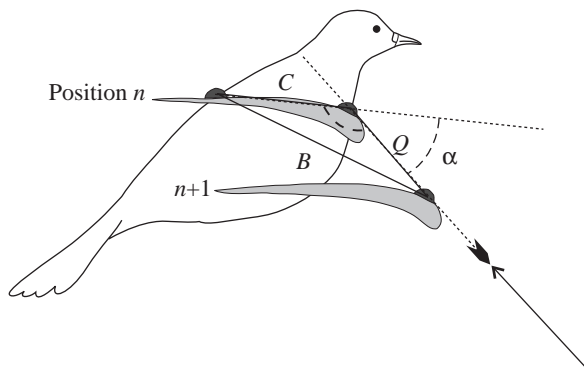
Fig. 3. Calculation of angle of attack ($\alpha$) using the angle of a line through the wing chord ($C$) relative to the path of the wrist through the laboratory coordinate space from position $n$ to $n+1$ ($Q$), and the distance ($B$) between the trailing-edge marker at position $n$ and the leading-edge marker at $n+1$. The vector of the incident air (small arrowhead) is the reciprocal of the path of the wrist (large arrowhead).

position $n$ to $n+1$ during the time interval $t$ (see the Appendix; equation A1). The scalar term 'speed' is used here rather than velocity as the above computation leaves the directional component of velocity ambiguous.

Angle of attack ($\alpha$) was defined as the supplement to the interior angle formed by the vertex of the vector of the relative incident air ($V_{ri}$) and the chord line of the airfoil (Fig. 3). In flapping flight, the incident air velocity is the sum of three air vectors: the velocity of the body ($V_b$), the velocity of flapping ($V_f$) and the induced velocity ($V_i$), the vector sum of wake and bound vortices on the wing. While $V_b$ and $V_f$ are subsumed in the changes in the laboratory coordinate position of the wing, in the present study, it was impossible to calculate an independent $V_i$ for each wing. As estimates of $V_i$ using Rankine–Froude momentum jet theory assumptions become poor when unsteady effects dominate, such as during slow flight (Aldridge, 1986), we chose to ignore induced velocity in our calculations of angle of attack. Flapping velocity and body velocity are the dominant vectors during flapping flight, although at low speeds, induced velocity becomes an important vector component and omitting it can produce large errors in estimation of angle of attack (Aldridge, 1986). While we here assume that $V_i$ is the same for both wings and that its effects would cancel out in a description of asymmetry in angle of attack between the two wings, inferences drawn using absolute angle of attack should be regarded with caution.

Using three-dimensional Pythagorean distances between coordinates, an instantaneous estimation of angle of attack was calculated as the interior angle formed by a line drawn between the wrist marker and the trailing-edge marker and the vector of the incident air created by the wrist movement (see Appendix, equations A2 and A3; Fig. 3).

Asymmetries in the surface area of the wing were inferred using the angle of wrist extension ($\varepsilon$) in the two-dimensional plane of the wing, which was defined as the interior angle of the triangle formed by the three wing markers on a wing, and calculated using the law of cosines (similar to equation A2). As the wing tips were usually visible for only 3–4 frames at mid-downstroke, asymmetries in surface area were sampled only at this time.

*Calculation of kinematic variables in the bird coordinate system: excursion, bank angle, downstroke velocity, pronation and downstroke angles*

To make inferences about the functional morphology of maneuvering flight, some variables required a kinematic frame of reference different from the laboratory coordinate system – namely, a frame of reference developed around the bird's body (henceforth termed the local coordinate system). This local coordinate system was created by the three coplanar body points. By translating and rotating the three body points (and, simultaneously, all other marker coordinates), the left body marker became the origin of the local coordinate system (i.e. point 0,0,0), with the right anterior body markers identifying the $xy$ plane, and an axis perpendicular to that plane identifying the $z$ dimension (Fig. 2A). The translation and rotation of the body markers resulted in the right body marker having the local coordinates ($x_\rho,0,0$), and the anterior marker having local coordinates ($x_\zeta,y_\zeta,0$), where $x_\rho$ was simply the Pythagorean distance between the right and left markers, and ($x_\zeta,y_\zeta$) was calculated trigonometrically from the relative positions of the right and left markers (see Appendix, equations A4–A14). Using the body markers, the angle of the lateral and longitudinal axes of the bird relative to the floor plane (i.e. bank and body angles) and the heading of the bird were extracted during the calculation of the local coordinate system as described in the Appendix. Subjecting all nine markers at each point $n$ to the three rotations (in the same order) constantly reset the body marker points as the $x$, $y$, $z$ coordinate system while keeping the relative positions of the six wing markers exactly the same as they were prior to translation and rotation. Thus, after translation and rotation into the bird coordinate system, movement of the wing markers during the time interval $t$ (5 ms) represents movement relative to the body. All discussions of wing excursion, downstroke velocity, pronation and downstroke angles will refer to variables computed in the bird coordinate system.

The velocity of the wing in the $x_l$ dimension (calculated similarly in the $y_l$ and $z_l$ dimensions) was calculated simply as the change in position in that dimension during the time interval $t$. Total downstroke and upstroke velocities were then calculated by the Pythagorean method (as in equation A1). We discriminate between upstroke and downstroke kinematics, with downstroke periods defined by a negative wrist velocity in the $z_l$-dimension of the local coordinate system, and upstroke as that period during which the wrist had a positive $z_l$ velocity. To eliminate ambiguous data points lying in the wing turn-around transition periods, data were not selected unless the wrist velocities were above an absolute value of $1.00\,\mathrm{m\,s^{-1}}$.

To investigate the possibility that asymmetries in pronation angles systematically occurred such that the birds would appear to be using angle of attack asymmetries in low-speed

maneuvering (Dial and Gatesy, 1993), we describe the pronation angle ($\delta$) through downstroke. Pronation was calculated as the amount of wing rotation in the $xy$ and $xz$ planes (see Appendix, equation A15). This sums the degree of ventral rotation of the wing regardless of its position during the downstroke and results in higher angular values when pronation is larger. For example, a positive pronation at mid-downstroke would occur when the $z$ position of the wrist was lower than that of the trailing edge (Fig. 2B).

Downstroke angle ($\lambda$) was calculated as the posterior angle formed by the wrist path and the longitudinal axis of the body (i.e. the $x$ axis in the bird coordinate system; Fig. 2C). This differs from the stroke plane angle (e.g. Scholey, 1982; Aldridge, 1986), which describes the overall movement of the wing through space (i.e. including its movement due to the motion of the entire bird). While stroke plane angle is thus a useful index in the estimation of the aerodynamic conditions surrounding the wing, downstroke angle only describes movement within the body's frame of reference, thereby providing insight into anatomical conditions (e.g. humeral excursion). An overall downstroke angle was calculated from the line drawn between the wrist positions at the beginning and end of the downstroke.

### Analyses of kinematic patterns

To determine the wing kinematic mechanisms that the birds used to maneuver, wrist downstroke and upstroke velocity (always left minus right), angle of attack ($\alpha$) and wrist extension angle ($\varepsilon$) were regressed against the change in bank and heading angle. Changes in bank and heading angle were calculated as the difference in those body orientations occurring immediately after the wing kinematic event. For example, the change in bank angle was calculated as the change from position $n$ to $n+1$; this change was then regressed as a dependant variable on the asymmetry in the velocity of the wrist as calculated from position $n-1$ to $n$. As the wing kinematic data were sequential, time-series autoregressive models (autoregression coefficient is abbreviated as ARC) were employed in the analyses.

In physical terms, the causal relationship we sought to establish was between inferred aerodynamic force asymmetry produced by the wing and the resulting angular acceleration ($a$) around a chosen body axis. The aforementioned autoregressive linear models using wing kinematic variables and body angular velocities in roll (i.e. change in bank angle) from point $n$ to $n+1$ were used as a first examinations of these relationships. Because acceleration data were much more erratic than velocity data, we

computed angular acceleration of the body as the change in the average angular velocity before and after the wing kinematic asymmetry. Downstrokes and upstrokes with more than four tracked points and those showing asymmetry to the same side for three points in a row were selected [given the error in the coordinate mapping, any small asymmetries ($<0.30\,\mathrm{m\,s^{-1}}$) that alternated in sign from point to point were considered unreliable; large asymmetries did not so fluctuate]. An average angular velocity in roll was calculated for the period just prior to the onset of the wing asymmetry and for the same number of points just after the wing asymmetry was observed. Angular acceleration in roll was then calculated as the change in angular velocity during the period of wing asymmetry.

Kinematic asymmetries often showed a pattern of reversal within a downstroke. To examine these patterns, we selected downstrokes that we were able to track for more than eight frames (35 ms; $N$=40). We defined reversal as a minimum of three consecutive points (10 ms) showing asymmetries in the same direction, followed by three consecutive points showing asymmetries in the opposite direction.

All kinematic and statistical calculations were performed using Microsoft Excel (version 5.0) or SPSS (version 7.0). Values are presented as means ± S.D.

## Results

### General descriptors

*Bank and heading angles, body pitch, flight speed and turning radius*

The saltatory nature of force production in flapping flight results in oscillating changes in the birds' bank and heading angles, flight speeds and rates of flight path curvature (Fig. 4). During downstroke, bank angles generally increased in the direction of the turn (e.g. in a right turn, right bank angle usually increased during downstroke). During upstroke, bank angles usually ceased to increase in the direction of the turn or decreased. The highest average angular velocity in roll was $33.09\,\mathrm{rad\,s^{-1}}$ ($1895\,^\circ\,\mathrm{s^{-1}}$) during the downstroke that also produced the highest angular acceleration ($2112.92\,\mathrm{rad\,s^{-2}}$) (Table 1) and change in bank angle ($49.26\,^\circ$). Even with such large angular accelerations (mean $601\pm465\,\mathrm{rad\,s^{-2}}$), 95 % of bank angle changes during downstroke were less than $30\,^\circ$. The changes in heading angle during downstroke were in the opposite direction to the direction of the changes in bank angle; for example, in a right bank, there was a significant tendency for the heading to change to the left (Fig. 5). This suggests that adverse yaw was produced during bank initiation.

Table 1. *Mean whole-body kinematics of three pigeons during turning flight*

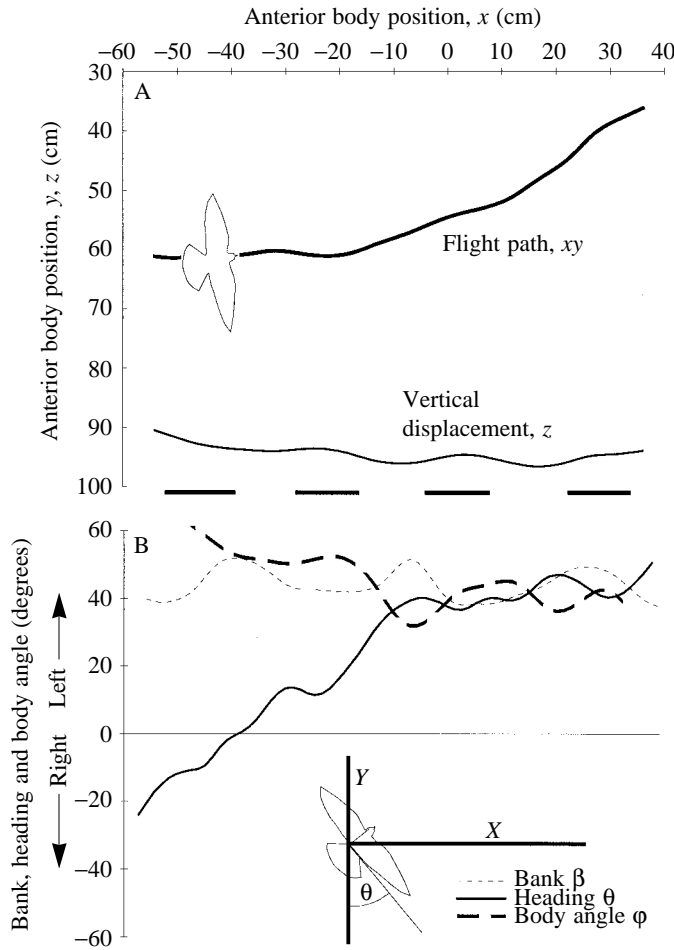|  | $N$ | Mean ± S.D. | Minimum | Maximum |
|---|---|---|---|---|
| Right turn bank angle (degrees) | 1880 | 25.0±15.0 | 39.0 | 70.7 |
| Left turn bank angle (degrees) | 944 | 32.1±11.2 | −4.27 | 78.1 |
| Angular acceleration in bank (rad s$^{-2}$) | 63 | 601±465 | 7.57 | 2113 |
| Body angle (degrees) | 386 | 33.59±14.37 | 8.90 | 74.99 |
| Flight speed (m s$^{-1}$) | 3887 | 2.87±0.61 | 1.38 | 5.96 |

Fig. 4. (A) Raw positional data of a pigeon making a left turn. Saltatory force production creates oscillations in the rate of curvature and height above floor. The illustrated bird is approximately 50 % actual size relative to the increments on the graph. Black bars indicate downstroke periods (both graphs). (B) Bank (β), heading (θ) and body (φ) angles through the same turn. Initially, the pigeon has a heading slightly to the right (negative angle values); the heading angle becomes positive as the bird begins to turn to the left (angle calculated as in inset).
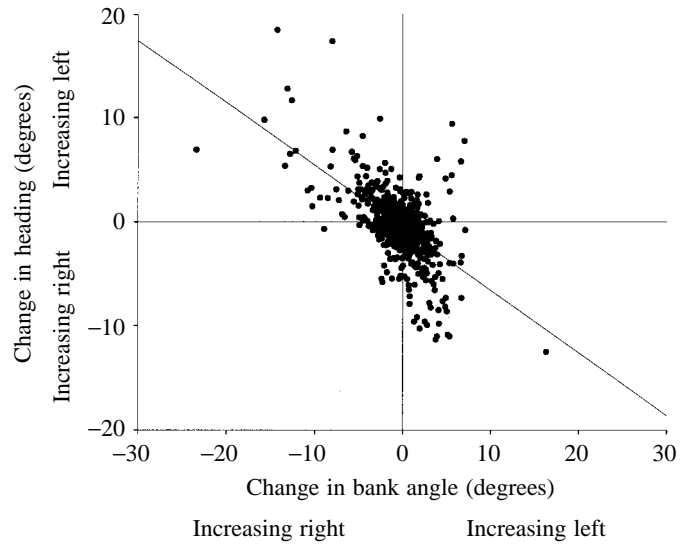


Fig. 5. Relationship between the change in heading and the change in bank angle. The negative correlation indicates the creation of adverse yaw during bank initiation. Data are sequential changes in angle from bank and heading sampled every 5 ms and are thus strongly autocorrelated. Autoregressive models were therefore used: ARC (=autocorrelation coefficient)=0.083, $N$=2936, $x$ coefficient=0.375, $r^2$=0.161, $P$<0.00001.

Mean body angle was 33.59±14.37 ° (Table 1) compared with the body angles of 36 ° reported by Tobalske and Dial (1995) for pigeons at 6 m s$^{-1}$. The mean flight speed of 2.87±0.61 m s$^{-1}$ was approximately half that reported in other studies of pigeon maneuvering in slow flight (Dial and Gatesy, 1993; Warrick *et al.* 1998), although a burst speed of nearly 6.00 m s$^{-1}$ was recorded. The average absolute bank angle (i.e. averaging both left and right turns) through the turns was 27.33±13.73 °, with a maximum of 78.08 ° and a minimum of −4.27 ° (a slight right bank during a left turn). The mean radius of a turn in the $xy$ plane was 1.46±0.66 m in right turns and 1.79±0.72 m in left turns.

Table 2. *Mean downstroke\* kinematics of three pigeons during turning flight*

|  | $N$ | Mean ± S.D. | Minimum | Maximum |
|---|---|---|---|---|
| Tip speed (m s$^{-1}$) | 67 | 8.27±3.72 | 3.08 | 24.3 |
| Wrist speed (m s$^{-1}$) | 214 | 4.00±1.16 | 1.15 | 8.02 |
| Wrist speed, upstroke* (m s$^{-1}$) | 113 | 2.56±0.80 | 0.70 | 4.23 |
| Angle of attack (degrees) | 191 | 34.6±7.42 | 12.7 | 53.8 |
| Wrist extension angle (degrees) | 749 | 90.6±10.1 | 13.5 | 165 |
| Downstroke angle (degrees) | 86 | 76.5±16.2 | 18.3 | 115 |
| Pronation angle (degrees) | 212 | 23.2±15.4 | −55.8 | 66.3 |
| Mean right-dominant asymmetry (m s$^{-1}$) | 555 | 1.32±1.32 | 0.00 | 7.65 |
| (mean as % of maximum) |  | (17.30%) |  |  |
| Mean left-dominant asymmetry (m s$^{-1}$) | 416 | 1.23±1.34 | 0.00 | 6.95 |
| (mean as % of maximum) |  | (17.6%) |  |  |

*Wrist speed during upstroke is given also.

Fig. 6. Raw local coordinate positional data ($z$ axis) and aerodynamic variables over time in one wingbeat cycle. A decrease in the local coordinate $z$ dimension represents the depression of the wing relative to the body (i.e. downstroke), while an increase in the $z$ dimension indicates that the wing was being raised (i.e. upstroke; indicated by arrow). A $z$ position of 0 cm indicates that the wing is at the same elevation as the body markers, or approximately mid-downstroke. Given a consistent vector of incident air, pronation angle would determine angle of attack. The decrease in pronation angle to values less than zero indicates that the wing is being supinated, in this case resulting in high angles of attack. As typically occurred, the trailing edge and wingtip markers were not in view of the cameras during upstroke and early downstroke, resulting in the gaps in pronation angle, angle of attack and wingtip data. Wrist speed (the term 'speed' is here used, as traces reflect only magnitude) and tip speed are direct derivations from local three-dimensional positional data. Note the protraction of tip downstroke and speed (and presumably, aerodynamic force production) beyond the end of wrist downstroke.
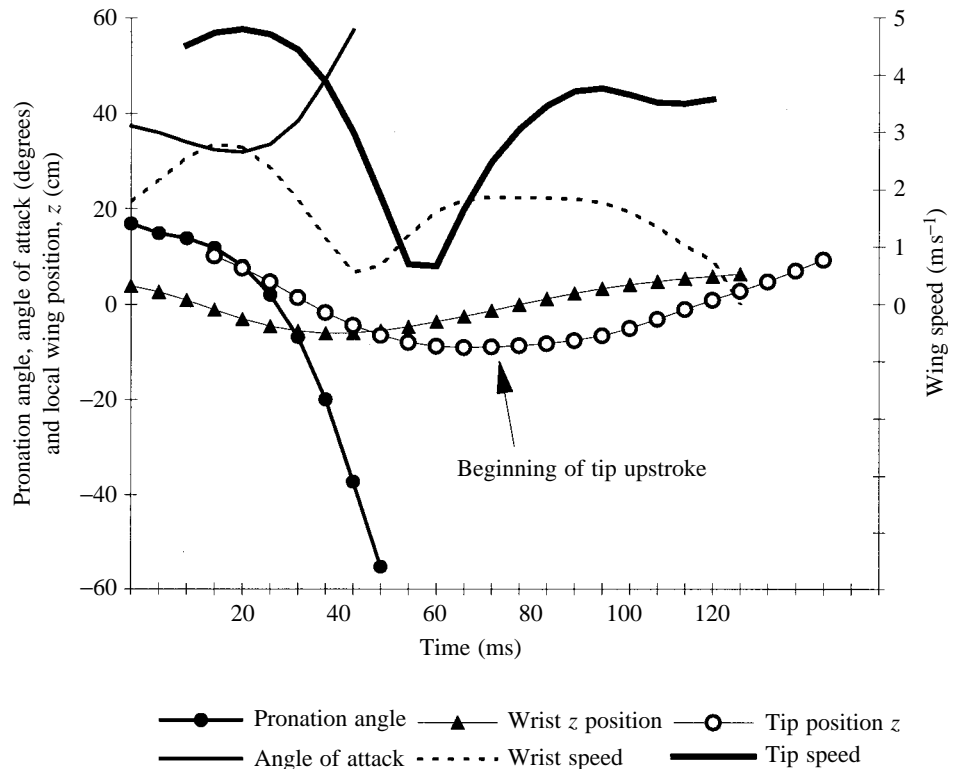
## Mean downstroke kinematics

As kinematic data will subsequently be presented as asymmetries, we here provide mean kinematic descriptors and brief qualifying discussions to give an immediate context within which to view those asymmetries (Table 2).

Mean downstroke tip and wrist velocities relative to the body were $8.27\pm3.72\,\mathrm{m\,s^{-1}}$ and $4.00\pm1.16\,\mathrm{m\,s^{-1}}$ respectively (Table 2). During the middle of the downstroke, wrist velocity was predictably half that of the tip, as the wrist marker had a radius of arc approximately half that of the tip marker (Fig. 6). At the end of humeral downstroke, however, tip velocity remained high ($>3.00\,\mathrm{m\,s^{-1}}$) while wrist velocity decreased rapidly with the end of humeral excursion (Fig. 6).

The pigeon's mean downstroke angle of attack at the wrist was $34.6\pm7.42°$ (Table 2). Aldridge (1986) observed downstroke angles of attack of approximately $45°$ for a horseshoe bat *Rhinolophus ferrumequinum* (mass 0.022 kg) flying at speeds nearly identical to those of our pigeons ($2.7\,\mathrm{m\,s^{-1}}$). As stated above, because we ignored induced velocity, our absolute values of measures of angle of attack are probably low (Aldridge, 1986).

The mean mid-downstroke wrist pronation angle was $23.2\pm15.4°$ (Table 2). Pronation angle was fairly constant during the middle 50 % of downstroke excursion, finally decreasing and becoming negative (by definition, supinated) at the end of the downstroke (Fig. 6). As the wrist was still being driven downwards at over $1\,\mathrm{m\,s^{-1}}$ (only these data were considered part of the downstroke), such supination sometimes

resulted in very high angles of attack (maximum $53.79°$; Table 2) probably stalling the proximal wing. Few other data exist for pronation angle of a bird wing during downstroke. Bilo (1971) observed a $20.1°$ pronation of the distal wing (7 cm from the shoulder joint, which is approximately the same as the pigeon's shoulder-to-wrist distance) in a free-flying house sparrow *Passer domesticus*.

The mean downstroke angle for all birds and all trials was $76.5\pm16.2°$ (Table 2), which is less than the $96°$ angle reported by Tobalske and Dial (1996) for pigeons in level flight at $6\,\mathrm{m\,s^{-1}}$. One extremely low minimum downstroke angle ($18.27°$) was observed, the result of an erratic, arrested downstroke where the bird appeared to lose track of its destination and hesitate during the turn around the barrier.

The mean wing wrist extension angle of $90.6\pm10.1°$ suggests that the hand-wing was generally fully extended during downstroke. However, we cannot dismiss the possibility that some flexion of the wrist occurred early in downstroke, as we were unable to track the wingtip markers during this portion of the wingbeat cycle. Angles of greater than $90°$ were produced by the multiaxial nature of the wrist joint (Vasquez, 1992); at the end of downstroke, the wrist is generally flexed downwards while still being extended in the plane of the wing (Brown, 1948; D. R. Warrick, personal observation), and the resulting angle measured in the three-dimensional laboratory coordinate system can exceed the extension angle of the wrist in the two-dimensional wing plane.

Mean wrist velocity during upstroke ($N$=113) was 2.56± 0.80 m s$^{-1}$ (Table 2).

### Patterns of asymmetry and changes in body position: angle of attack, downstroke/upstroke velocity and downstroke angle

Change in bank angle was highly correlated with wrist downstroke velocity asymmetry (Fig. 7A). A change in bank angle was usually preceded by a higher wrist downstroke velocity on the outside wing: a higher wrist downstroke velocity on the right preceded an increasing bank to the left, and a higher wrist downstroke velocity on the left preceded an increase in right bank angle. There was a strong linear correlation between average wrist downstroke velocity asymmetry and average angular acceleration in roll (Fig. 7B). The mean asymmetry in downstroke velocity was 1.28±1.32 m s$^{-1}$ (Table 2, averaging the absolute value of all asymmetries, left- and right-dominant).

Conversely, greater wrist downstroke velocity on the wing on the outside of the turn was strongly correlated with a change in heading angle (Fig. 8A) and angular acceleration opposite to the presumed intended direction of flight (Fig. 8B). For example, a greater wrist downstroke velocity on the right frequently produced a heading change to the right. Recall that heading θ is the angle between the laboratory coordinate $y$ axis and the right and left body markers on the bird (Fig. 4B; see Appendix; equations A5–A7), and that negative headings indicate a right-hand turn through the laboratory coordinate system, and positive headings indicate turns to the left. Assuming an average bank of 34°, changes in the heading angle must have, in part, resulted from some rotation around the yaw axis of the bird projected onto the laboratory $xy$ plane (i.e. the floor). This result suggests that the larger downstroke velocity on the outside wing, and resultant higher drag, produced an adverse yawing moment.

Autoregressive models show a significant tendency for the outside wing to have a higher downstroke angle than the inside wing (Fig. 9) during those downstrokes that result in a change in bank angle. A higher downstroke angle means that the path of the downstroke was more perpendicular to the longitudinal axis ($x$) of the bird's body.

Contrary to our expectations of higher angles of attack on the outside wing just prior to bank angle changes, a regression of asymmetry in angle of attack on the change in bank angle and the angular acceleration in bank revealed no such tendency (change in bank angle: $N$=805; $r^2$=0.000; ARC=0.816; angle of attack asymmetry coefficient=0.011; $P$=0.201; angular acceleration: $N$=62; angle of attack asymmetry coefficient=0.000; $r^2$=0.024; $P$=0.116). Similarly, no correlation was found between wrist downstroke angle asymmetry and change in bank angle ($N$=213; $r^2$=0.000; ARC=0.308; wrist angle asymmetry coefficient=−0.024; $P$=0.317).

We also found no relationship between asymmetry in pronation angle at mid-downstroke and change in bank angle ($N$=100; $r^2$=0.000; ARC=0.350; pronation angle asymmetry coefficient=−0.007; $P$=0.454). It should be noted here that the
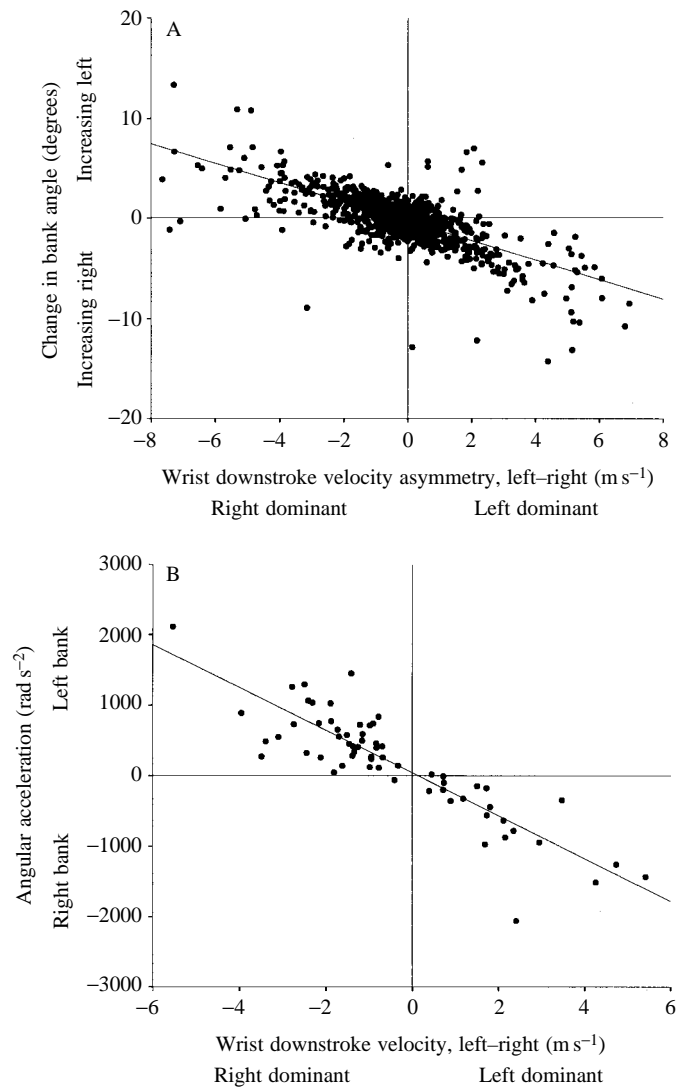


Fig. 7. (A) Relationship between the change in bank angle (i.e. angular velocity) and the wrist downstroke velocity asymmetry immediately preceding it. The correlation indicates the creation of roll following velocity asymmetry. $N$=969, ARC=0.775, $x$ coefficient=0.008, $r^2$=0.505, $P$<0.0001. (B) Angular acceleration in bank (averaged over approximately 20 ms) *versus* the asymmetry in wrist velocity immediately preceding it. $N$=63, $x$ coefficient=−3.024, $r^2$=0.760, $P$<0.001.

inferred angle of attack asymmetries observed by Dial and Gatesy (1993) occurred very early in the downstroke, a portion of the wingbeat cycle we were unable to track in the present study.

Pronation angle and downstroke angle were positively correlated. The angle of pronation increased with increasing downstroke angle (right wing: $N$=72; ARC=0.224; pronation coefficient=0.295; $r^2$=0.034; $P$=0.007; left wing: $N$=88; ARC=0.326; pronation coefficient=0.715; $r^2$=0.094; $P$=0.004), although little of the variance was accounted for by linear models. Higher pronation angles with higher downstroke angles presumably reflected the bird pronating the wing into
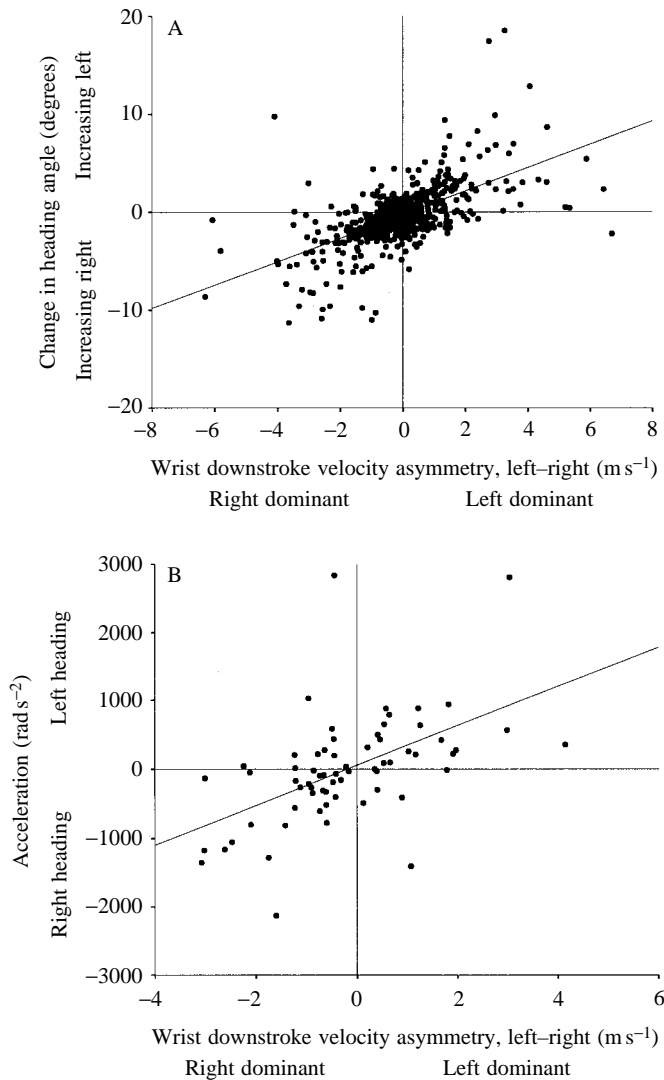
Fig. 8. (A) Relationship between the change in heading angle and wrist downstroke velocity asymmetry. $N=650$, ARC=0.750, $x$ coefficient=0.007, $r^2=0.370$, $P<0.0001$. (B) Angular acceleration in heading with wrist velocity asymmetry, illustrating the production of adverse yaw. $N=65$, $x$ coefficient=2.89, $r^2=0.270$; $P<0.0001$.
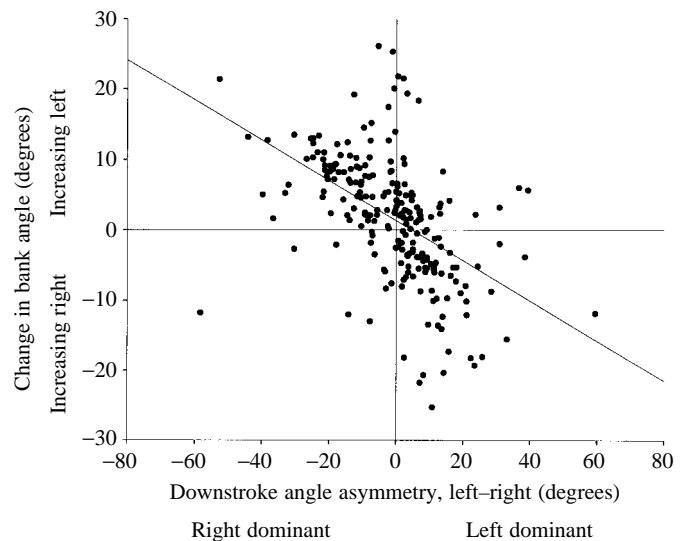


Fig. 9. Asymmetry in downstroke angle *versus* the change in bank angle. During a downstroke that creates a change in bank angle, the outside wing (which has a higher downstroke velocity; see Fig. 7A) has a higher downstroke angle. A higher downstroke angle means that the path of the wing was more nearly perpendicular to the $x$ axis of the bird coordinate system; angles greater than $90°$ mean that some portion of the wrist movement was in the caudal direction. $N=226$, ARC=0.548; $x$ coefficient=−0.195; $r^2=0.257$; $P<0.0001$.

the direction of the more ventrally originating incident air created by the increased downstroke angle, thus maintaining a consistent angle of attack

### Patterns of wrist velocity asymmetry within a downstroke

The method of creating kinematic asymmetry bears directly on the efficacy of the torque created in producing rolling angular accelerations (see Discussion). To determine whether the pigeons were creating velocity asymmetries by a velocity reduction on the inside wing or by an increase in velocity on the outside wing, we regressed the absolute magnitude of wing velocity asymmetry between positions $n$ and $n+1$ against the sum of the right and left velocities during the same period. If the birds were reducing the velocity on the inside wing, the summed velocity would be statistically independent of the absolute magnitude of the velocity asymmetry. Alternatively, if the pigeons were creating asymmetry by increasing the velocity on the outside wing, the summed velocity would increase with increasing absolute magnitude of asymmetry. Using autoregressive models, the latter case was found to be true ($N=966$; ARC=0.6432; summed velocity coefficient=0.211; $r^2=0.107$; $P<0.0001$). In general, the birds created asymmetry by producing greater-than-average velocity on the outside wing.

Examination of the wrist velocity asymmetries within a downstroke revealed a strong pattern of reversed downstroke wrist asymmetries within the same wingbeat; that is, birds created a wrist velocity asymmetry in the early portion of downstroke, and then created an opposite asymmetry in the later portion of the same downstroke. Such a reversal occurred in 28 of 40 (70%) of downstrokes (Fig. 10). Taking an average of wrist velocity asymmetries from before and after reversal, regression analysis revealed that the asymmetries created at the end of the downstrokes were highly negatively correlated with the strength of the asymmetries created early in the downstrokes (Fig. 11).

In 13 of the 28 reversals (46%), the pigeons began the downstroke with an asymmetry that caused them to increase their bank angle in the direction of flight (e.g. increase right bank angle during a right turn), and then reversed the asymmetry to arrest or reverse their angular momentum (Fig. 12). Of the 15 reversals in which the birds led with an asymmetry that reduced their bank angle, 11 (76%) occurred during trials conducted after the flight course direction had

Fig. 10. Reversing wrist downstroke velocity asymmetries within a downstroke. The $x$ axis for all graphs is time, with each increment the equivalent of 5 ms. (A) A downstroke velocity asymmetry beginning with the right wing dominant and ending with the left wing dominant. The first fraction of the downstroke was not in view of the cameras (the first $z$ position recorded for the wrist is 2 cm, indicating that the wing was just above mid-downstroke), but the beginning asymmetry was clearly right-wing-dominated; the higher velocity of the right wing results in a lower wrist position in the $z$ dimension for the right wing when it first comes into view. The left wing then increases in downstroke velocity, until the asymmetry reverses (note that, in this example, the right wrist marker left the view of the cameras before the right wing reached mid-downstroke). Note that the bank angle initially increases to the left (higher positive values) and then reverses to the right as the left wing begins to dominate. (B) Birds frequently exhibited similar asymmetry reversal patterns in sequential wingbeats. (C) In this example, the first downstroke ends with a left-dominant asymmetry and resulting increasing right bank. During upstroke, however, the bank angle changes rapidly to a slight left bank. Given the direction of the asymmetry at the end of the previous downstroke, this change in bank angle during the first upstroke (between the dotted lines) could only be a product of upstroke mechanisms.
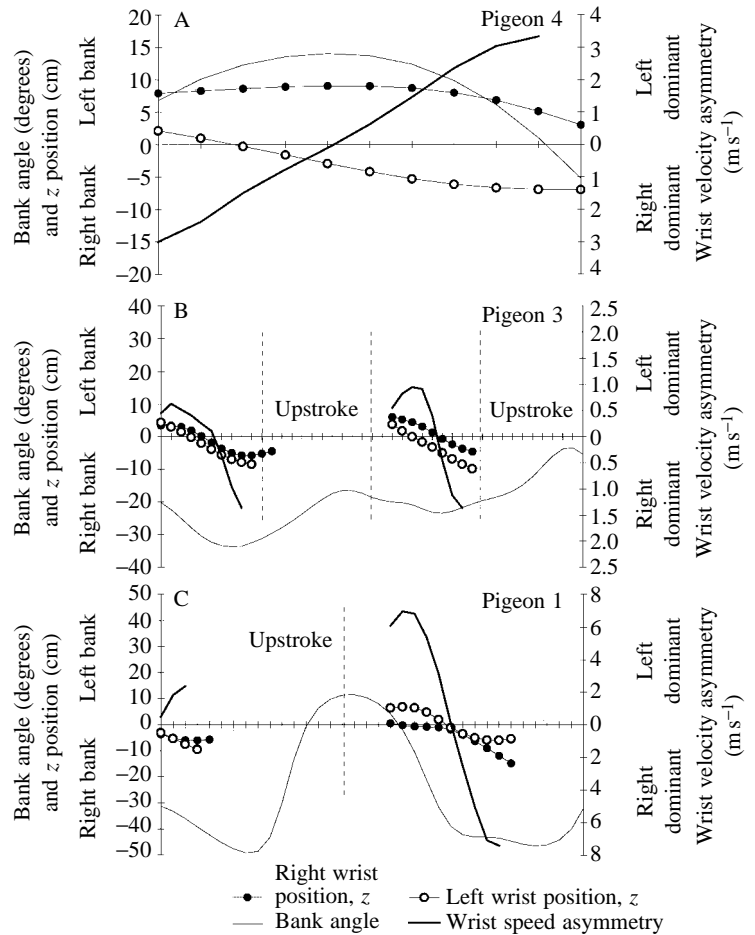
been switched. This suggests that the birds became accustomed to turning in the direction first presented.

Of the 40 downstrokes examined for reversal, 12 (30 %) did not show asymmetry reversal. Six of these 12 created higher bank angles (henceforth termed 'initiating' downstrokes) and six created reduced bank angles ('recovery' downstrokes). The lack of wrist velocity asymmetry reversal in the initiating downstrokes suggested a need for force reversal after the end of downstroke to prevent the bird from over-banking. We were only able to track (through to the next downstroke) five of the six unreversed downstrokes that had initiated banking. In two of these five cases, the angular momentum produced by the downstroke asymmetry was reversed during the next upstroke (see below); in two others, the momentum was reversed during the next downstroke. The remaining asymmetry was small (0.27 m s$^{-1}$) and resulted in no change in bank angle.

### Wrist velocity asymmetries during upstroke

The arrest of otherwise unchecked angular momentum produced during the previous downstroke and the pronounced changes in bank angle that frequently occurred during upstroke (17 % of wingbeat cycles; Fig. 10A) suggested that this phase of the wingbeat cycle was actively involved in producing force asymmetries. To investigate further the possibility that force asymmetries were being produced during upstroke and used to
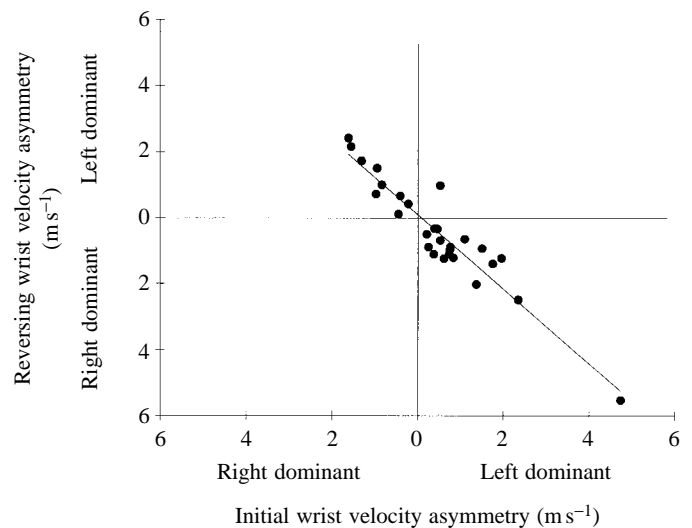


Fig. 11. Within a downstroke, the magnitude of the reversing asymmetry was strongly correlated with the magnitude of the initiating asymmetry. When a bird produced a velocity asymmetry at the beginning of a downstroke ($x$ axis), it produced an approximately equal and opposite asymmetry later in the same downstroke ($y$ axis) to arrest the momentum created by the initial asymmetry. $N=15$, $x$ coefficient=$-0.976$, $r^2=0.856$, $P<0.0001$.
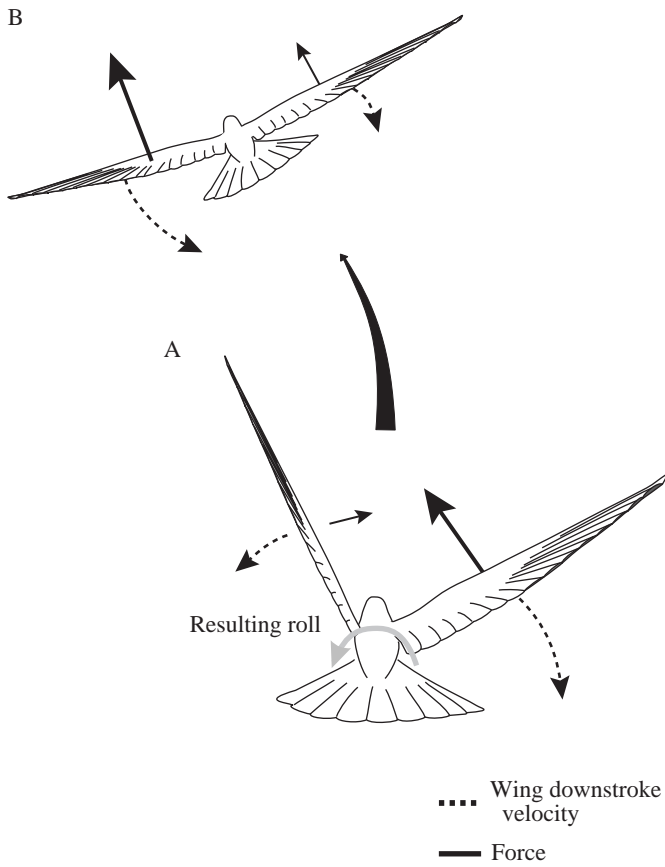
Fig. 12. (A) Representation of a pigeon using velocity (dashed arrows) asymmetry early in downstroke to initiate banking (grey arrow), and (B) reversing the velocity asymmetry later in the same downstroke to arrest the banking momentum. The solid arrows depict the relative size of the aerodynamic forces resulting from the respective downstroke velocities.
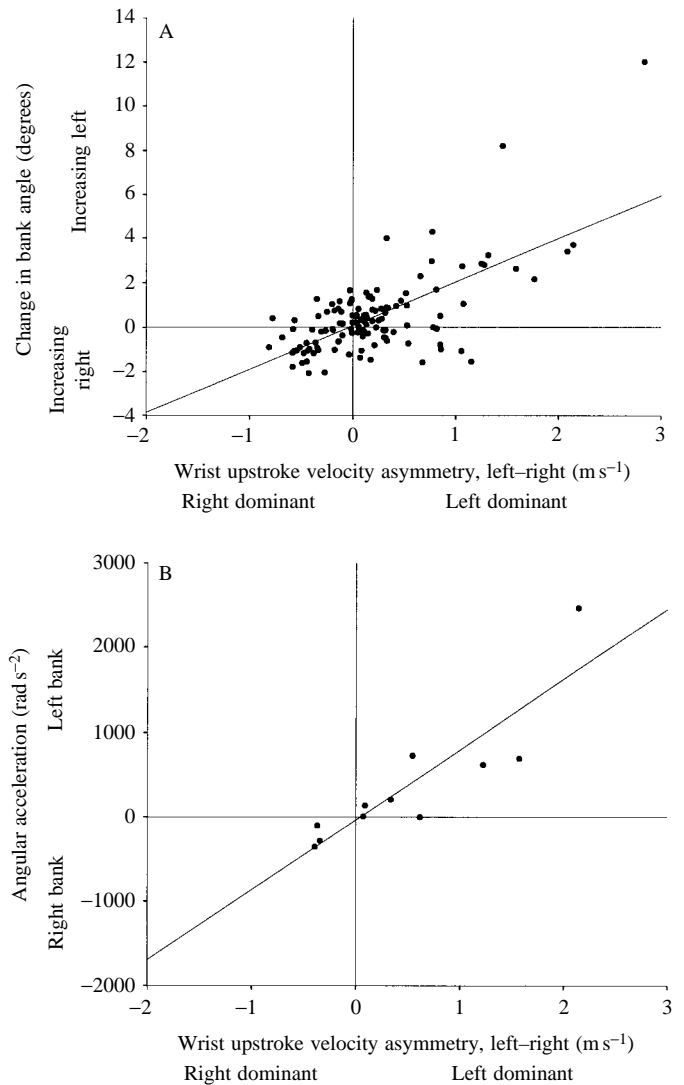


Fig. 13. The change in bank angle (A) and the angular acceleration in bank (B) with wrist upstroke velocity asymmetry. The positive slopes of the relationships indicate that the direction of the force asymmetry is opposite to that in the downstroke; that is, that the force employed is produced by drag. (A) $N$=126, ARC=0.629, $x$ coefficient=0.023, $r^2$=0.446, $P$<0.0001. (B) $N$=10, $x$ coefficient=8.278, $r^2$=0.754, $P$<0.0001.

arrest rolling momentum, we examined 13 (the two mentioned above, plus 11 others) tracked upstrokes where roll was initiated or the roll created during the previous downstroke was reversed (i.e. upstrokes in which angular acceleration was produced). The 11 additional upstrokes were not used in the analysis in the previous section as their preceding downstrokes were not fully tracked. The correlation between upstroke wrist velocity asymmetry and the change in bank angle and angular acceleration (Fig. 13) clearly suggests that upstroke was used actively to alter body orientation. The positive slopes of these regressions indicate that the forces produced by the wings during the upstroke had a direction opposite to those produced during downstroke – that is, the forces produced in the upstroke were developed by drag.

### *The use of kinematic asymmetries: an extreme example*

To illustrate the potential of the above kinematic mechanisms, Fig. 14 presents traced images (high-speed light film, 300 frames s$^{-1}$) of a pigeon traveling at approximately 3 m s$^{-1}$ recovering from a human-induced inverted position (180 °). Although initially rolled 180 ° to the left, the pigeon has rotated

its head to keep it upright, presumably to maintain a frame of reference. Before the downstroke, the wings were held symmetrically above the midline of the body (frame 1), as in a typical downstroke. As the downstroke begins, the right wing is immediately flexed (probably to reduce its inertia), lowered and strongly pronated, possibly to reduce its angle of attack to the incident air produced by the strong rolling movement (frame 2). Little, if any, lift would seem to be produced, and the right wrist appears to be in a much lower position relative to the body than the left. The left wing is still high in the *z* dimension and being driven powerfully down, producing a large velocity asymmetry between the two wings. The right wing is held flexed and pronated until the end of the left wing's
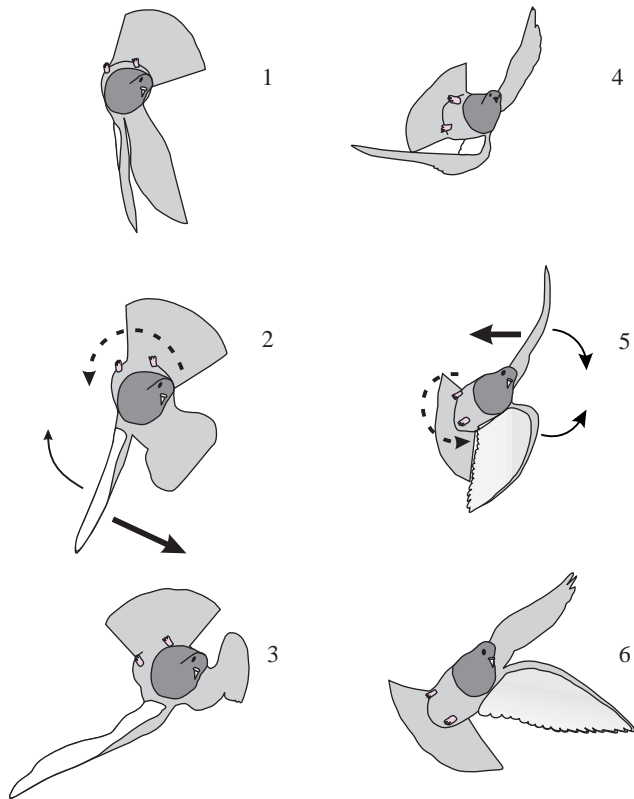
Fig. 14. Traced images from high-speed film (300 frames s$^{-1}$) of a pigeon (*Columba livia*) recovering from a handler-induced inverted position. The pigeon had been gently tossed from the hand (<3 m s$^{-1}$) while held inverted. Frames are 12 ms apart. The bird clearly uses velocity (and excursion) asymmetries during the downstroke; thin arrows are wing movement, and heavy arrows are inferred lift forces (2) and drag forces (5). Dashed arrows depict the direction of body roll. Through downstroke velocity asymmetry, excursion asymmetry and the use of the upstroke, the pigeon rolls approximately 135° in approximately 50 ms.

downstroke, at which time the right wing, having been through a downstroke excursion of zero, is again fully extended and raised quickly in upstroke (frames 4 and 5). The ventral bending of the feathers indicates that a drag force is being produced (Boel, 1929; Brown, 1948); in this case, the direction of the force would serve to roll the bird further to the right, continuing its recovery. Note that the upstroke of the left wing is more typical, with the wrist strongly flexed and the wing supinated (frame 5).

## Discussion

In terms of the simple physics of locomotion, the use of force asymmetries in the downstroke to produce bank changes and effect a turn during the critical stages of low-speed flight may be counterintuitive. Aerodynamically, lift varies with the square in velocity, thus squaring the force-production effects of any unintentional asymmetry in downstroke. Conversely, the linear changes in lift with changes in angle of attack (i.e.

lift coefficient) and wrist flexion (wing surface area) and the muscles responsible for making such alterations would seem to be ideally suited for producing such effects. Why, then, are these fine-scale anatomical mechanisms and their aerodynamic mechanisms not employed, rather than the relatively brutish pectoralis and its velocity mechanism? Several non-exclusive possibilities present themselves. (1) At low speeds, there are anatomical, kinematic and/or aerodynamic limits to flapping flight that preclude the use of changes in angle of attack or surface area. In addition, the neuromuscular organization needed for the large-scale recruitment and high power output (Clarke, 1931; Henneman *et al.* 1965) of the pectoralis may prevent it from creating fine-scale asymmetries in velocity. The result is the creation of fine control of locomotion by juxtaposition of large-scale mechanisms. (2) The lift forces involved are intrinsically not strong enough ever to produce dramatic changes in body position, even if great asymmetry exists. Finally, (3) using mechanisms that produce intrinsically large forces is, in fact, the safest way to maneuver at low speeds (or at any speed, for that matter).

### The use of velocity asymmetries: anatomical constraints on the use of pronation and flexion, and implications for the evolution of the pectoralis

Altering wing pronation and the lift coefficient may not be a desirable strategy during slow flight because the bird may be using the wing near the kinematic and aerodynamic limits of these mechanisms, thus limiting the options for altering them. However, with the mean downstroke pronation angle of 23° and an observed maximum of 66°, it would seem that the birds in the present study were not at a kinematic limit in terms of their abilities to alter angle of attack. Increasing the lift coefficient from the mean value may not have been an option, however, as the mean angle of attack was extremely high (>35°) and the lift coefficient was probably close to maximum during most downstrokes. However, the pigeons clearly had the anatomical latitude to pronate more strongly and reduce the lift coefficient during downstroke, and such reductions would theoretically be sufficiently effective. The mean wrist downstroke velocity asymmetry observed was approximately one-quarter that of the mean downstroke speed, which would result in the inside wing producing only half as much lift as the outside wing. Assuming no downstroke velocity asymmetries and a linear decrease in lift coefficient with decreasing angle of attack, a bird should be able to produce a similar force asymmetry by halving its angle of attack and lift coefficient by simply pronating to 40°. Similarly, flexing the wrist to an angle of 30° would reduce the hand-wing surface area by 50% (modeling the area of the primaries as a triangle) and reduce lift proportionately.

Finding no proximal physical reason for not creating angular accelerations with flexion or pronation, the simplest explanation for why birds do not use these mechanisms is that they do not wish to reduce downstroke lift at low altitude. Because of the unsteady nature of weight support force production by the downstroke (owing to the direction of the vector, the

aerodynamic force produced during upstroke would not provide much weight support), birds must not only maintain altitude with the downstroke but also recover the height they lost during the upstroke (several centimeters; Fig. 4A).

We should stress that the apparent lack of systematic use of angle of attack in low-speed maneuvering flight does not mean that anatomical mechanisms such as pronation are not important. Angle of attack and downstroke velocity are closely related; as downstroke velocity changes, the wing must be rotated to adjust its presentation to the changing direction of the incident air. For example, if the wing increases in velocity in the *z* dimension, it would need to be pronated more strongly in the *xz* plane to maintain the same angle of attack. The fact that downstroke velocity was routinely varied but angle of attack was not suggests active modification of wing presentation through pronation and supination to maintain a useful incident air angle. The mechanisms involved are not clearly understood, although muscle stimulation studies demonstrate the potential for the use of the biceps and triceps (Dial and Gatesy, 1993). In addition, the insertion of the pectoralis on the ventral side of the delto-pectoral crest provides ideal leverage for strong pronation of the humerus, and thus the entire wing. As the strength of this pronation would increase with increasing pectoral downstroke force (and hence downstroke velocity), the insertion of the pectoralis on the delto-pectoral crest may provide a means of automatically rotating the leading edge of the wing into the incident airstream, thus maintaining a useful angle of attack. Such an automatic mechanism would be a kinematic strategy similar in principle to the linkage system that automatically extends the wing at the elbow and the wrist during the downstroke (Headley, 1895; Fisher, 1957; Dial, 1992*b*; Vasquez, 1994).

The presence of such automatic mechanisms raises the possibility of anatomical restrictions on the use of flexion and pronation at low flight speeds. With regard to the automatic linkage system, it may take complex, powerful neuromuscular activity to flex the wing throughout a strong downstroke typical of slow flight. Similarly, the insertion of the pectoralis on the delto-pectoral crest may automatically set an angle of attack during the downstroke, which the bird would need to alter actively using some other mechanism (pronators/supinators, biceps/triceps, flexors; Dial and Gatesy, 1993). In short, altering wing area or angle of attack may be a more complicated neuromuscular proposition than altering downstroke velocity – particularly during portions of the downstroke where high aerodynamic forces are being generated. Yet, given the sophistication of the remainder of the wingbeat cycle, it should not be an anatomically impossible proposition.

A pigeon's ability to create sequential, precisely opposing wrist velocity asymmetries in the same downstroke (a 50 ms kinematic event) clearly indicates that the role of the pectoralis in low-speed maneuvering flight is much more than just the production of high mass-specific power. Studies of the physiology and neural control of the pectoralis (Dial *et al.* 1987, 1988; Dial, 1992*a*; Kaplan and Goslow, 1989; Boggs

and Dial, 1993) have illustrated the sophistication and multi-role potential of this muscle. The partitioning of the pectoralis into neuromuscular compartments and differences in the timing of recruitment in these regions as the downstroke progresses during different modes of level flight (Dial *et al.* 1987; Dial, 1992*a*; Boggs and Dial, 1993) hint at possible mechanisms underlying the ability to create rapidly reversing asymmetries during downstroke. Further, differences in recruitment patterns of these regions undoubtedly underlie the differences in downstroke angle seen between the two wings during bank initiation. For example, the more vertical and slightly posterior movement during the outside wing downstroke (i.e. high downstroke angle) may be the result of increased recruitment of the thoracobrachialis head of the pectoralis, which has been implicated in the retraction of the humerus (Dial *et al.* 1988).

In summary, discussions of the evolution of the pectoralis (and hence flapping flight) must address not only the power required (e.g. Peterson, 1985) but also the importance of the control of that power during low-speed maneuvering. Studies of the regional activity and contractile properties of the pectoralis during maneuvering flight may shed considerable light on the biomechanical function and evolution of this extrordinary muscle.

### The role of the supracoracoideus in low-speed maneuvering

The use of upstroke velocity asymmetries to create angular accelerations of the body illustrates that the major upstroke muscle, the supracoracoideus (Dial *et al.* 1988), may have evolved not simply in response to the demands of stereotypical wing recovery but also in response to the demands of fine-scale maneuvering (see Poore *et al.* 1997). While there has long been good evidence that some aerodynamic force is produced during upstroke, the kinematic data presented here provide the first evidence that birds use those forces purposefully during locomotion. Boel (1929) suggested that the inverted primaries may produce lift during upstroke, while others (Brown, 1948; Norberg, 1976; Aldridge, 1986) have suggested that propulsive force may be produced from drag-based mechanisms. Whatever the case, the force produced during upstroke would be less than that produced with an equal velocity asymmetry during downstroke. The lift coefficient of a cambered airfoil at a negative angle of attack would be much lower than that of the same airfoil at a positive angle. Similarly, the drag coefficient of feathers that bend backwards to a more streamlined position during upstroke would be lower than if the feathers were cupped forwards, as during downstroke. Combined with the smaller velocity-generating ability of the supracoracoideus (mean upstroke velocity at the wrist was 64 % of mean downstroke velocity), the aerodynamic forces produced by the upstroke would probably be less than 50 % of those generated by the downstroke. However, the reduced effectiveness of upstroke asymmetry may not be a liability; indeed, it may make it well-suited to provide additional fine-scale control during low-speed maneuvering.

One further means by which the the supracoracoideus might

be involved in maneuvering flight is its activity at the end of downstroke. Just prior to manus inversion, the hand-wing is driven forwards and upwards as the wrist is ventrally flexed and the wing supinated, probably resulting in a slight (<10 ms) protraction of lift generation. Velocity asymmetries in this portion of the downstroke could be generated by differential activity of the forearm supinators (e.g. M. supinator) or the supracoracoideus supinating the entire wing.

### Stability in slow flight and the strength of downstroke aerodynamic forces

The intrinsic stability of a bird in flight is a function the moment of inertia of the body relative to the forces generated by the wings during locomotion. Given the inertia of a bird in slow flight, are the powerful forces generated by velocity asymmetries more 'appropriate' than those that could be generated by pronation or flexion? Norberg and Rayner (1987) describe rolling performance as the ratio of the torque available from lift relative to the inertia of the wings and body. Similarly, Srygley and Dudley (1993) describe the maneuvering performance of moths as a function of the moments of inertia of their bodies. However, a flying animal's inertia is proportional to the square of its radius of gyration ($r$), the average distance from the axis of rotation to the mass being moved, and this axis may change according to the mode of flight and type of bank initiation.

The three traditional axes of rotation for a flying machine are roll, yaw and pitch (Fig. 2A). Modeling the body as a uniform cylinder of length $K$, transverse radius $r_r$ and longitudinal radius $r_l$, the moments of inertia ($I$) of a body with mass $m$ rotating around these three axes can be estimated as $I_{roll}=\frac{1}{2}mr_r^2$ and $I_{yaw}=I_{pitch}=\frac{1}{4}m(r_l^2+K^2/3)$. Thus, for a pigeon with a body that is twice as long as it is thick, the moment of inertia in the yaw or pitch axes would be approximately 2.5 times that in the roll axis. The moments of inertia for the wings would be approximately the same in any of these axes; hence, more torque (force asymmetry multiplied by its moment arm) would be needed to produce an angular acceleration in the yaw and pitch axes than in the roll axis.

In higher-speed flight, because of the higher velocity of the incident air from the movement of the body ($V_b$), the vector sum of the velocity of the incident air will be closer to parallel to the longitudinal axis of the body than at low speeds (Fig. 15A), as long as downstroke speeds are relatively low (e.g. at intermediate speeds; Dial *et al.* 1997). To maintain a useful angle of attack at high speeds, the pronation angle of the wing should thus be lower than that during slow flight (this has indeed been found to be the case for zebra finches *Taenopygia guttata*; B. Tobalske, personal communication). This lower pronation angle will direct a larger component of the lift force perpendicular to the roll axis of rotation and would make the bird intrinsically more unstable (Fig. 15A). Conversely, with the high pronation angles of slow-speed flight, more lifting force would be directed perpendicular to the yaw axis of rotation, thus making the bird intrinsically more stable (Fig. 15B).
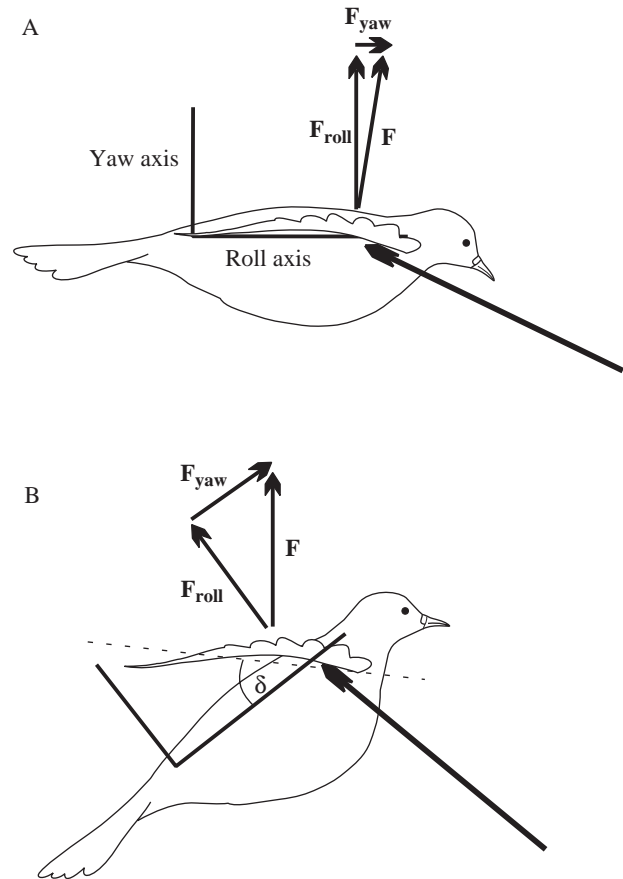


Fig. 15. (A) In level flight at higher speeds, the pronation angle ($\delta$) of the wing during downstroke should be relatively low, as the direction of the incident air is more aligned with the longitudinal axis of the bird. This would result in a large portion of the lift vector (**F**) from the wings being directed perpendicular to the roll axis (**F$_{roll}$**). (B) At low airspeeds, the wing is more strongly pronated (dotted line is through chord of wing), directing more of the total lift force perpendicular to the yaw axis (**F$_{yaw}$**). Given the higher moment of inertia of the bird around the yaw axis (relative to the moment of inertia around the roll axis; see Discussion), the bird flying at low speed would be intrinsically more stable.

A final inertial mechanism that may dampen the effects of downstroke force asymmetry is simply the continued force production on the inside wing. The aforementioned moment of inertia in the roll axis is a description of a roll around the center of the bird's mass – henceforth termed a 'rotational roll'. Such a roll would be produced only if no lift were generated on the inside wing, as in the illustrative case of the pigeon recovering from an inverted position (Fig. 14) and in Fig. 16A. In the slow, maneuvering flights observed in the present study, rolls were rarely performed in this manner. Instead, the pigeons initiated bank by producing an average downstroke velocity on the inside wing and greater-than-average velocity on the outside wing. By creating excess lift on the outside wing while still producing weight-supporting lift on the inside wing, the lifting force of the inside wing will act as the point of rotation (i.e. the fulcrum) of the roll, resulting in a vertical and
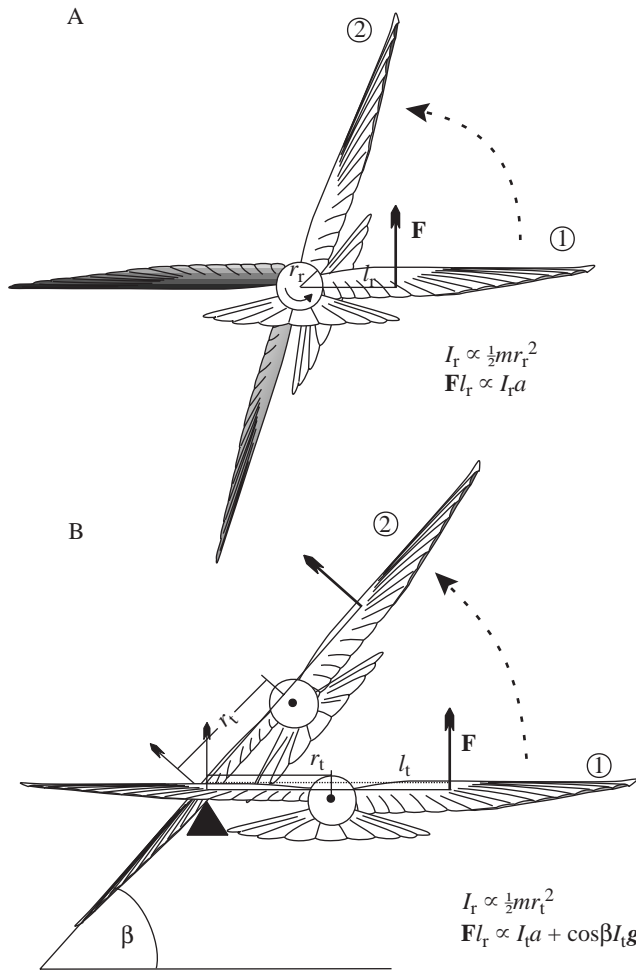
A



$$I_r \propto \tfrac{1}{2}mr_r^2$$
$$\mathbf{F}l_r \propto I_r a$$

B

$$I_r \propto \tfrac{1}{2}mr_t^2$$
$$\mathbf{F}l_r \propto I_t a + \cos\beta I_t \mathbf{g}$$

Fig. 16. The moment of inertia ($I$) of a banking bird depends on the method of bank initiation. (A) If weight support lift is not developed on the inside wing (at high speed, this would require, as represented by the shaded inside wing, pronation of the wing to a zero or negative angle of attack or completely folding the wing), the bird will roll around its center of mass ('rotational roll'), which has a relatively low moment of inertia ($I_r = \tfrac{1}{2}mr_r^2$, where $m$ is body mass, $a$ is acceleration, $r_r$ is the radius of gyration around the center of mass with the bird's body modeled as a cylinder). The torque accelerating this inertia would be the lifting force $\mathbf{F}$ times the moment arm $l_r$. (B) If weight-supporting lift (small arrow on left wing) is maintained on the inside wing, it will act as a fulcrum (black triangle) around which the body will move translationally as well as rotationally ('translational roll'). In this case, at any instant during a bank angle ($\beta$) less than $90\,^{\circ}$, the torque (lifting force $\mathbf{F}$ times lever arm $l_t$) created by the wing's force asymmetry will not only be accelerating the inertia of the body ($I_t = m$ times the square of the radius of gyration in translational roll $r_t^2$) but also opposing the inertia's acceleration due to gravity ($\mathbf{g}$).

horizontal (i.e. translational, hence 'translational roll') movement of the body (Fig. 16B). The moment of inertia of the bird's body (the wings could be similarly included) engaged in a translational roll can be described as $mr_t^2$, where $r_t$ is the distance between the fulcrum produced by the inside wing and the bird's body. The torque $\mathbf{F}l_t$ (force $\mathbf{F}$ times lever

arm $l_t$) produces an angular acceleration ($a$); additionally, however, the force must be equal to the body's moment of inertia multiplied by its acceleration due to gravity ($\mathbf{g}$). The moment of inertia that is subjected to gravitational acceleration changes as a function of the change in its radius as the bird banks; at any instant, it will be a function of the cosine of the bank angle $\beta$.

Although a bird in slow flight is probably intrinsically more stable than during high-speed flight, the pigeons in the present study were capable of producing extremely high angular velocities ($>30\,\mathrm{rad\,s^{-1}}$) and accelerations ($>2000\,\mathrm{rad\,s^{-2}}$) during slow flight, demonstrating clearly that at any given instant, the forces involved were more than adequate to produce strong (potentially catastrophic) body movements. However, even in employing what would seem to be fairly high angular accelerations, 95 % of all bank angle changes were less than $30\,^{\circ}$. In summary, while strong locomotor mechanisms were used and rapid oscillations in body position and flight path resulted, on the whole, the flights were steady, controlled events.

### The use of high-force mechanisms during maneuvering flight

Pronation and flexing mechanisms are used to great effect in the high-speed maneuvering flight of pigeons, swallows (Hirundidae) and nighthawks *Chordeiles minor* (Brown, 1948; Warrick, 1994) and have been implicated in the maneuvering flight of pigeons at more intermediate speeds ($6\,\mathrm{m\,s^{-1}}$, Dial and Gatesy, 1993). Furthermore, at $6\,\mathrm{m\,s^{-1}}$, pigeons were seen to use downstroke asymmetries to augment force asymmetry for the production of large angular accelerations (Dial and Gatesy, 1993), as has also been observed in bats flying at similar speeds (Norberg, 1990). The exclusive use of downstroke velocity at low speed, the possible combination of all three mechanisms at intermediate speeds and the use of the lift coefficient and wing area mechanisms at high speeds suggest that birds are, in fact, using the most effective means available during maneuvering at all speeds. At high speeds, twisting the wings to produce angle of attack asymmetries can be initiated immediately, without any preparation (i.e. an upstroke). In addition, by not driving the wings through a downstroke while pronating/supinating, the bird directs most of the lift on the outside wing perpendicular to the roll axis, and could theoretically produce negative angles of attack on the inside wing. The result would be a pure-rotation bank, with the bird rolling around its center of mass at high angular accelerations.

The idea (and resulting unsupported hypothesis) that birds should use fine-scale physical mechanisms (pronation/supination, flexion) during slow flight probably stemmed from the lack of a critical piece of information regarding maneuvering flight: how, and more importantly *when*, do birds halt the angular momentum created during bank initiation? The alien temporal scale at which birds operate weakens our intuitive sense of their locomotion; although extreme to our experience, the high rolling angular accelerations birds use in low-speed maneuvering (mean $>600\,\mathrm{rad\,s^{-2}}$) can produce precise locomotion if they are arrested (or reversed) immediately. In essence, a bird is

creating a precise path through space by 'averaging' a series of alternating gross movements.

A bird's use of the most effective mechanisms available to it during critical stages of flight makes the most sense when it is considered within the full context of aerial locomotion. Unlike terrestrial species, aerial species are routinely faced with strong vagaries in their locomotor substrate. The inconsistent nature of air and the relatively low inertia of birds may require them to make constant, authoritative adjustments to their position, especially on take-off and landing. Pilots of aircraft would immediately recognize the advantage of more positive control at low speed; as the speed of the aircraft diminishes relative to any wind present, the path of the aircraft over the ground becomes dominated by the direction of that wind. Becoming more 'planktonic' as one approaches the runway (or a perch) can quickly erode the utility of flight, and the development of aerodynamic mechanisms that can provide positive control at low speeds has been the focus of many aeronautical engineers. So, too, must it have been the focus of natural selection.

## Appendix

*Body movement and wing kinematic calculations from three-dimensional coordinates*

### Airspeed

Airspeed $S$ is given by:

$$S = \frac{\sqrt{(Ax_{n+1} - Ax_n)^2 + (Ay_{n+1} - Ay_n)^2 + (Az_{n+1} - Az_n)^2}}{t} , \quad (A1)$$

where $A$ is the coordinate position of the anterior body marker in each of the three dimensions ($x$, $y$, $z$) in the sequence of sampled positions $n$ to $n+1$, and $t$ is the sampling time interval.

### Angle of attack

Angle of attack $\alpha$ is given by:

$$\alpha = 180 - \left( \cos^{-1} \frac{(Q^2 + C^2 - B^2)}{2QC} \right), \quad (A2)$$

where $Q$ is the distance between the trailing edge marker and the wrist marker, $C$ is the distance between the wrist position $n$ and $n+1$, and $B$ is the distance between the trailing edge marker at $n$ and the wrist marker at $n+1$. The above angle of attack was adjusted ($\alpha_a$) by subtracting the angle created by the elevation of the marker. As the position of the wrist marker was 1 cm above the true chord line,

$$\alpha_a = \alpha - \sin^{-1}(1/C). \quad (A3)$$

All discussions of angle of attack refer to this adjusted estimate ($\alpha_a$).

### Euler angle rotations: creating the local coordinate system ($x_l, y_l, z_l$) and calculating bank, heading and body angles

Translation of the three body markers and six wing markers from their laboratory coordinates to local coordinates required subtracting the $x$, $y$ and $z$ laboratory coordinate positions of the left marker ($L$) at each point in the series $n$ from the coordinates of all nine markers at the same point in time. For example, for translating the right tip ($RT$) to ($RT_T$):

$$RT_{T(x,y,z)} = RT_{(x,y,z)} - L_{(x,y,z)}, \quad (A4)$$

and so on for all eight other markers.

With the left body marker now at point (0,0,0) and all eight other points still in their same relative positions, a series of three Euler angle rotations was computed, such that, for each point in the path, the right body marker would rotate to $x=0$ and $z=0$, and the anterior body marker to $z=0$. The first (I) rotation was about the $z$ axis, rotating through an angle $\theta$ to bring the right body marker ($R$) to local $x=0$ by rotating it by $\theta$ degrees ($\theta = R_x/R_y \tan^{-1}$), where $R_x$ and $R_y$ are the translated right body marker coordinates in the $x$ and $y$ dimensions. Subjecting all nine marker points to the first rotation (I), the resulting coordinates for each were:

$$x_I = x\cos\theta - y\sin\theta, \quad (A5)$$

$$y_I = x\sin\theta + y\cos\theta, \quad (A6)$$

$$z_I = z. \quad (A7)$$

The angle $\theta$ is the angle of this $z$ axis rotation projected onto the $xy$ laboratory coordinate plane (i.e. the floor), and it thus describes the heading of the bird in the laboratory coordinate system. It was subsequently used in analyses relating kinematic asymmetries to changes in body position. Note that a negative heading indicates turning to the right, positive indicates turning to the left.

The second (II) rotation was about the $x$ axis through an angle $\beta$ ($\beta = R_z/R_y \tan^{-1}$), bringing the right body marker to $z=0$:

$$x_{II} = x_I, \quad (A8)$$

$$y_{II} = y_I\cos\beta + z_I\sin\beta, \quad (A9)$$

$$z_{II} = y_I\sin\beta + z_I\cos\beta. \quad (A10)$$

The angle $\beta$ also describes the bird's bank angle relative to the floor at a given instant and was used in subsequent analyses. Again note that right bank angles are given as negative values, left bank angles as positive.

The final (III) Euler angle rotation through an angle $\gamma$, about the $y$ axis ($\gamma = A_z/A_x \tan^{-1}$) brings the anterior body marker to $z=0$:

$$x_{III} = x_{II}\cos\gamma + z_{II}\sin\gamma, \quad (A11)$$

$$y_{III} = y_{II}, \quad (A12)$$

$$z_{III} = x_{II}\sin\gamma + z_{II}\cos\gamma. \quad (A13)$$

Coordinates $x_{III}$, $y_{III}$ and $z_{III}$ are now complete local coordinates, renamed $x_l$, $y_l$ and $z_l$. Because of the previous rotation around the $x$ axis, $\gamma$ is no longer an accurate representation of the longitudinal body angle of the bird to the horizontal (henceforth, 'body angle'). Body angle ($\varphi$) was calculated from laboratory coordinates as:

$$\varphi = \frac{(A_z - L_z)}{\sqrt{(A_y - L_y)^2 + (A_x - L_x)^2}} \ \tan^{-1} . \qquad (A14)$$

*Pronation angle*

Pronation angle $\delta$ is given by (e.g. for the right wing):

$$\delta = \frac{\sqrt{(RR_{y_l} - RW_{y_l})^2 + (RR_{z_l} - RW_{z_l})^2}}{(RR_{x_l} - RW_{x_l})^2} \ \tan^{-1} , \quad (A15)$$

where *RR* is the right wing trailing edge local coordinate position and *RW* is the right wing wrist local coordinate position.

## List of symbols

| | |
|---|---|
| *a* | acceleration |
| *A* | anterior body marker |
| *B* | distance from trailing edge at *n* to leading edge at *n+1* |
| *C* | wing chord distance |
| **F** | lift force vector |
| **F$_{roll}$** | lift force vector perpendicular to roll axis |
| **F$_{yaw}$** | lift force vector perpendicular to yaw axis |
| *g* | acceleration due to gravity |
| *I* | moment of inertia |
| *I$_{pitch}$* | moment of inertia around a traditional pitch axis |
| *I$_r$* | moment of inertia in a rotational roll |
| *I$_{roll}$* | moment of inertia around a traditional roll axis |
| *I$_t$* | moment of inertia in a translational roll |
| *I$_{yaw}$* | moment of inertia around a traditional yaw axis |
| *K* | cylinder length |
| *l$_r$* | lever arm of lifting force in rotational roll |
| *l$_t$* | lever arm of lifting force in translational roll |
| *L* | left body marker |
| *LR* | left trailing edge marker |
| *LT* | left wingtip marker |
| *LW* | left wrist marker |
| *m* | body mass |
| *n* | number in a series |
| *n+1* | next number in a series |
| *Q* | distance from leading edge at *n* to leading edge at *n+1* |
| *r* | radius of gyration |
| *r$_l$* | cylinder longitudinal radius |
| *r$_r$* | cylinder transverse radius; radius of gyration in a rotational roll |
| *r$_t$* | radius of gyration in a translational roll |
| *R* | right body marker |
| *RR* | right trailing edge |
| *RT* | right tip marker |
| *RT$_T$* | right body marker after translation |
| *RW* | right wrist marker |
| *S* | whole-body airspeed |
| *t* | time interval |
| **V$_b$** | bird velocity |
| **V$_f$** | flapping velocity |
| **V$_i$** | induced velocity |
| *V$_{ri}$* | relative incident air velocity |
| *x, y, z* | three-dimensional laboratory coordinates |
| *x$_\rho$* | fixed local *x* coordinate position of the right body marker |
| *x$_\zeta$, y$_\zeta$* | fixed local *x* and *y* coordinates of anterior body marker |
| *x$_{I–III}$, y$_{I–III}$, z$_{I–III}$* | *x, y, z* coordinates through Euler angle rotations |
| *x$_l$, y$_l$, z$_l$* | three-dimensional local coordinates |
| $\alpha$ | angle of attack |
| $\alpha_a$ | adjusted angle of attack |
| $\beta$ | bank angle |
| $\delta$ | pronation angle |
| $\gamma$ | third Euler rotation angle |
| $\varepsilon$ | wrist extension angle |
| $\varphi$ | body angle |
| $\lambda$ | downstroke angle |
| $\theta$ | heading angle |

## References

ALDRIDGE, H. D. J. N. (1986). Kinematics and aerodynamics of the Greater Horseshoe Bat (*Rhinolopus ferrumequinum*) in horizontal flight at various flight speeds. *J. exp. Biol.* **126**, 479–497.

BILO, D. (1971). Biophysics of the flight of small birds. I. Kinematics and aerodynamics of the downstroke of the House Sparrow (*Passer domesticus*). *Z. vergl. Physiol* **71**, 382–454.

BOEL, M. (1929). Scientific studies of natural flight. *Trans. Am. Soc. mech. Eng.* **51**, 217–242.

BOGGS, D. F. AND DIAL, K. P. (1993). Neuromuscular organization and regional EMG activity of the pectoralis in the pigeon. *J. Morph.* **218**, 43–57.

BROWN, R. H. J. (1948). The flight of birds: the flapping cycle of the pigeon. *J. exp. Biol.* **25**, 322–333.

CLARKE, D. A. (1931). Muscle counts of motor units: A study in innervation ratios. *Am. J. Physiol.* **56**, 296–304.

DIAL, K. P. (1992a). Activity patterns of the wing muscles of the pigeon (*Columba livia*) during different modes of flight. *J. exp. Zool.* **262**, 357–373.

DIAL, K. P. (1992b). Avian forelimb muscles and nonsteady flight:

Can birds fly without using the muscles in their wings? *Auk* **109**, 874–885.

DIAL, K. P., BIEWENER, A. A., TOBALSKE, B. W. AND WARRICK, D. R. (1997). Direct assessment of mechanical power output of a bird in flight. *Nature* (in press).

DIAL, K. P. AND GATESY, S. M. (1993). Neuromuscular control and kinematics of the wings and tail during maneuvering flight. *Am. Zool.* (Abstr.) **33**, 5.

DIAL, K. P., KAPLAN, S. R., GOSLOW, G. E., JR AND JENKINS, F. A., JR (1987). Structure and neural control of the pectoralis in pigeons: Implications for flight mechanics. *Anat. Rec.* **218**, 284–287.

DIAL, K. P., KAPLAN, S. R., GOSLOW, G. E., JR AND JENKINS, F. A., JR (1988). A functional analysis of the primary upstroke and downstroke muscles in the domestic pigeon (*Columba livia*) during flight. *J. exp. Biol.* **134**, 1–16.

FISHER, H. I. (1957). Bony mechanism of automatic flexion and extension in the pigeon's wing. *Science* **126**, 446.

HEADLEY, F. W. (1895). *Structure and Life of Birds*. London: Macmillan.

HENNEMAN, E., SOMJEN, G. AND CARPENTER, D. (1965). Excitability and inhibitability of motoneurons of different sizes. *J. Neurobiol.* **28**, 599–620.

KAPLAN, S. R. AND GOSLOW, G. E. (1989). Neuromuscular organization of the pectoralis (pars thoracicus) of the pigeon (*Columba livia*): Implications for motor control. *Anat. Rec.* **224**, 426–430.

MOTION ANALYSIS CORPORATION (1991). *Expert Vision User's Manual*. Santa Rosa, CA: Motion Analysis Corp.

NORBERG, U. M. (1976). Aerodynamics, kinematics and energetics of horizontal flight in the long-eared bat (*Plecotus auritus*). *J. exp. Biol.* **65**, 179–212.

NORBERG, U. M. (1990). *Vertebrate Flight: Mechanics, Physiology, Morphology, Ecology and Evolution*. Berlin: Springer-Verlag.

NORBERG, U. M. AND RAYNER, J. M. V. (1987). Ecological morphology and flight in bats (Mammalia; Chiroptera): Wing adaptations, flight performance, foraging strategy and echo-location. *Phil. Trans. R. Soc. Lond. B* **316**, 335–427.

PETERSON, A. (1985). The locomotor adaptations of *Archaeopteryx*: glider or cursor? In *The Beginnings of Birds. Proceedings of the International* Archaeopteryx *Conference Eichstätt*. Willibaldsburg: Freunds des Jura-Museums Eichstätt.

POORE, S. O., SANCHEZ-HAIMAN, A. AND GOSLOW, G. E., JR (1997). Wing upstroke and the evolutin of flapping flight. *Nature* **387**, 799–802.

RAYNER, J. M. V. (1988). Form and function in avian flight. In *Current Ornithology*, vol. 5 (ed. R. F. Johnston), pp. 1–66. New York: Plenum Press.

SCHOLEY, K. D. (1982). Developments in vertebrate flight: climbing and gliding of mammals and reptiles and the flapping flight of birds. PhD thesis, University of Bristol.

SRYGLEY, R. B. AND DUDLEY, R. (1993). Correlations of the position of the center of body mass with butterfly escape tactics. *J. exp. Biol.* **174**, 155–166.

TOBALSKE, B. W. AND DIAL, K. P. (1996). Flight kinematics of black-billed magpies and pigeons over a wide range of speeds. *J. exp. Biol.* **199**, 263–280.

VASQUEZ, R. J. (1992). Functional osteology of the avian wrist and the evolution of flapping flight. *J. Morph.* **211**, 259–268.

VASQUEZ, R. J. (1994). The automating skeletal and muscular mechanisms of the avian wing (Aves). *Zoomorph.* **114**, 59–71.

WARRICK, D. R. (1994). Flight morphology, performance and prey capture in a guild of aerial insectivores. *Am. Zool.* (Abstr.) **34**, 5.

WARRICK, D. R., DIAL, K. P. AND BIEWENER, A. A. (1998). Asymmetrical force production in the maneuvering flight of birds. *Auk* (in press).